Research article

JGS
Journal of the Geological Society

https://doi.org/10.1144/jgs2022-008 | Vol. 179 | 2022 | jgs2022-008

Thermal history of the southern Antarctic Peninsula during Cenozoic oblique subduction

G. Twinn[1]*, T. Riley[2], M. Fox[3] and A. Carter[1]

[1] Department of Earth and Planetary Sciences, Birkbeck, University of London, Malet Street, London WC1E 7HX, UK
[2] British Antarctic Survey, High Cross, Madingley Road, Cambridge CB3 0ET, UK
[3] Department of Earth Sciences, University College London, Gower Street, London WC1E 76BT, UK
GT, 0000-0003-4133-5926
*Correspondence: g.twinn@ucl.ac.uk

Abstract: Apatite (U–Th)/He and apatite fission-track thermochronology is used to constrain the cooling and uplift history of the southern Antarctic Peninsula where easterly-directed subduction of the Phoenix Plate, including ridge–trench collisions, has been taking place along its western margin since the Late Cretaceous. Apatite ages and thermal history models are similar on eastern Palmer Land but are younger and vary across westernmost Palmer Land and Alexander Island. Transformation of thermal history models to a single plot shows how cooling rates varied as a function of distance from the trench zone. Eastern Palmer Land preserves a record of uplift during the Late Cretaceous that coincides with changes in Phoenix Plate convergence rates and direction. In contrast, western Palmer Land and Alexander Island experienced a period of increased rates of cooling between *c.* 25 and 15 Ma. This younger phase of exhumation is bounded by major fault zones related to the extension and rifting that formed the present-day George VI Sound. It was probably triggered by cessation of subduction owing to trench collision of a ridge segment NE of the Heezen fracture zone. No evidence was found for slab window influences as seen along the northernmost part of the Antarctic Peninsula.

Supplementary material: QTQt thermal models, a PDF with analytical protocols and supplementary tables are available at https://doi.org/10.6084/m9.figshare.c.6086234

Received 17 January 2022; **revised** 13 June 2022; **accepted** 17 June 2022

The Antarctic Peninsula is a significant topographic feature, rising from an average elevation of 900 m at its northern tip to an average elevation of 1800 m some 800 km to the south. The elevated spine of the Antarctic Peninsula has a major impact on regional climate and acts as an orographic barrier that probably drove regional ice sheet nucleation (Siegert 2008). However, the timing and mechanism of uplift along the Peninsula remain poorly resolved, especially for its southern part. Marine sedimentary records indicate evidence of alpine glaciation along the Antarctic Peninsula as early as *c.* 37–34 Ma (Anderson *et al.* 2011; Wellner *et al.* 2011) suggesting that significant topography must have existed prior to this. This is also supported by recent thermochronometry work along the northern Peninsula (Clinger *et al.* 2020).

For more than 200 myr easterly-directed subduction has taken place along the western margin of the Antarctic Peninsula. From the Late Cretaceous this involved southeastward oblique subduction of the now extinct Phoenix Plate (also known as the Aluk or Drake Plate) and convergence of the Antarctic Plate. This resulted in strain partitioning within the forearc region accompanied by strike-slip motion and extension. Throughout the Cenozoic, subduction along the Peninsula ceased progressively from the SW to NE as a result of a series of Antarctic–Phoenix ridge–trench collisions (Larter and Barker 1991). The dynamic effects of the spreading ridge subduction on the geology of the overriding plate would have affected upper-plate topography and regional stress regimes but understanding is largely based on predictions from analogue modelling studies (e.g. Martinod *et al.* 2013; Salze *et al.* 2018). These show that show ridge–trench collision drives uplift of the overriding plate close to the forearc area along with flexural subsidence in the hinterland, and that over time the uplifted area migrates inland away from the trench–forearc region as slab dips shallow. However, many factors could affect this trend and the pattern of strain partitioning including variations in thickness and composition of the overriding plate, development of slab windows and rates of oblique convergence.

Many consider that surface uplift along the entire Peninsula may be explained by these near-orthogonal to the continental margin ridge crest–trench collision events, possibly facilitated by a migrating slab window and associated asthenospheric buoyancy (Larter and Barker 1991; Hole *et al.* 1994; Thorkelson 1996; Eagles *et al.* 2009). This was supported by an apatite thermochronometry study of the northern Antarctic Peninsula that detected systematic spatial trends in apatite cooling ages and a transgressive pulse of *c.* 2–3 km of rock uplift consistent with progressive Late Cenozoic northward opening of a slab window that followed ridge–trench collision (Guenthner *et al.* 2010). However, this may not be the case for the southern Peninsula, as the geology is different and there is a greater distance between the trench zone and the topographic spine compared with the northern Peninsula owing to Alexander Island, which is separated from the southern Antarctic Peninsula by a Cenozoic rift system that forms the present-day George VI Sound (Constantino *et al.* 2020).

It has been suggested that elevation growth along the southern Peninsula may be related to Late Paleogene rifting in the George VI Sound area and the formation of a triple junction (Storey *et al.* 1996*a*). Offshore Alexander Island ridge crest–trench collision, between the Tharp and Heezen fracture zones (Fig. 1), broadly took place between *c.* 50 and 30 Ma. Outcrop and seismic evidence of normal faulting and transtension shows that the George VI Sound formed by rifting during the Cenozoic (Bell and King 1998) but the nature of the extension is debated. Storey *et al.* (1996*b*) suggested

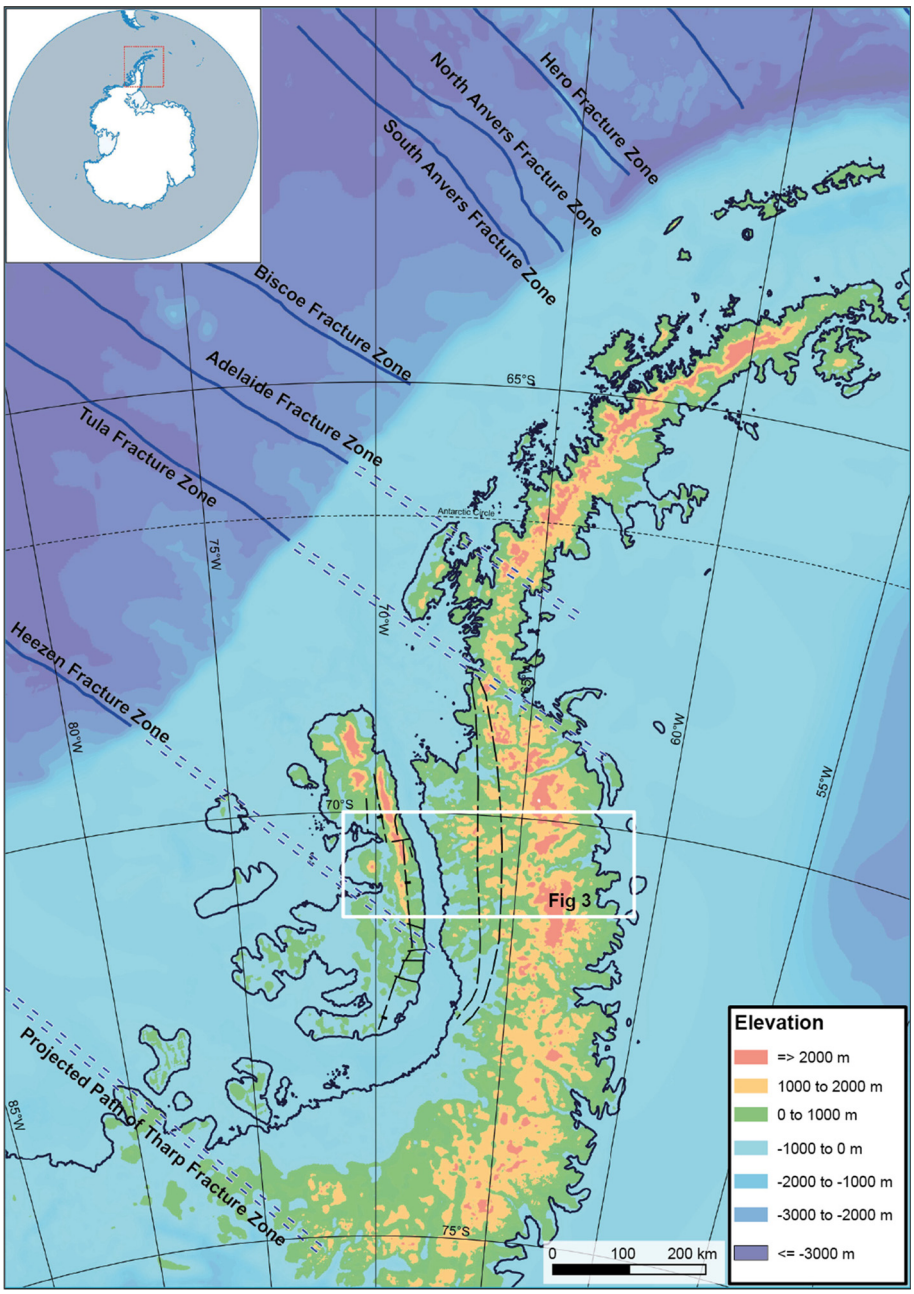

Fig. 1. Topography (ice removed) of the Antarctic Peninsula and relationship to location of former fracture zones. Elevation data are from Bedmap2 (Fretwell *et al.* 2013). Fracture zones are after Barker (1982) with their projected paths shown as dashed lines. Black dashed lines are fault zones after Bell and King (1998).

that the formation of a triple junction, as the spreading ridge that terminated at the Heezen Fracture zone was subducted, caused the thinning that allowed the rift to form. In contrast, Bell and King (1998) suggested that rifting could be the result of transtension caused by the cessation of subduction, causing the forearc basin formations on Alexander Island to detach from the edge of the Antarctic Peninsula Batholith. Modelling studies have shown that when a slab breaks off and forms a slab window there is a trench retreat effect on the overriding slab, which switches from a compressional to a tensional regime (Lallemand *et al.* 2005; Stegman *et al.* 2006; Salze *et al.* 2018). If there was significant trench retreat, then the main part of the Peninsula (arc and backarc) would experience the greatest deformation and normal faulting. To test these models and constrain the spatio-temporal patterns of rock cooling and exhumation we conducted an apatite fission-track and (U–Th)/He thermochronometry study using samples collected as a transect across Alexander Island and Palmer Land (southern Antarctic Peninsula) (Fig. 1).

Geology of the southern Antarctic Peninsula

The geology of the Antarctic Peninsula (Fig. 2) is dominated by an Andean-type continental arc with pulses of magmatism spanning the Ordovician to Eocene (Burton-Johnson and Riley 2015). One of the most significant magmatic pulses developed during the Early–Middle Jurassic and was related to rifting and mantle-plume activity associated with Gondwana break-up (Leat *et al.* 1995; Riley and Leat 2021) after which renewed subduction led to a period of crustal growth with arc, forearc and back-arc sequences forming in an extensional setting. Peak magmatism during this phase took place between *c.* 120 and 90 Ma and coincided with the development of the East Palmer Land Shear Zone. This shear zone is a major tectonic feature up to 20 km wide and over 1500 km long, and displays dextral-reverse deformation (Vaughan and Storey 2000; Vaughan *et al.* 2012) (Fig. 3). Alexander Island, situated on the western, forearc side of the Antarctic Peninsula, is dominated by a Mesozoic accretionary complex, termed the LeMay Group. The

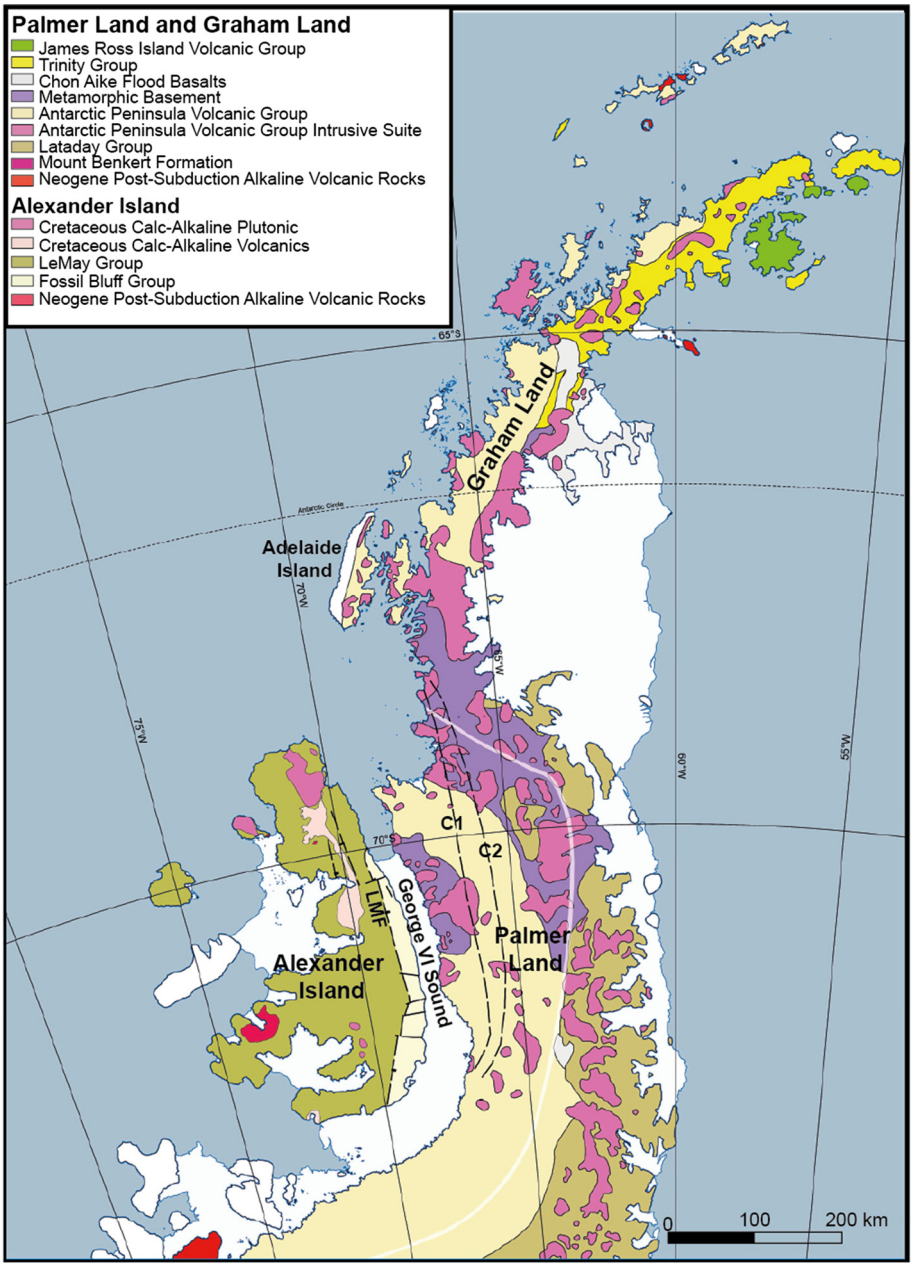

Fig. 2. Simplified geological map of the Antarctic Peninsula after Doubleday *et al.* (1993), Leat *et al.* (1995), Vaughan and Storey (2000), Crame *et al.* (2006), Hunter and Cantrill (2006), Hunter *et al.* (2006), Riley *et al.* (2011), Burton-Johnson and Riley (2015) and Castillo *et al.* (2015). LMF (LeMay Range Fault) and C1 and C2 faults are after Bell and King (1998).

easternmost boundary of the LeMay Group is bounded by the LeMay Range Fault, a strike-slip fault that extends roughly north–south (Fig. 2) that originally formed as a dextral strike-slip fault owing to the oblique subduction of the Phoenix Plate (Storey and Nell 1988). This fault separates the LeMay Group from the Mid-Jurassic to mid-Cretaceous Fossil Bluff Group (Doubleday *et al.* 1993), deposited in a forearc basin setting (Butterworth *et al.* 1988). The Fossil Bluff Group is intruded and partly overlain by Cretaceous calc-alkaline rocks. Alexander Island also hosts one of the largest occurrences of post-subduction basalts within the Antarctic Peninsula, but these significantly post-date the ridge crest–trench collision age (Hole 1988).

In the area of this study, spanning the Heezen fracture zone (Fig. 1), collisions between the Antarctic–Phoenix ridge segments and the former trench along the Antarctic Peninsula margin span *c.* 44–30 Ma (Larter *et al.* 1997). It is during this interval that subduction-related rifting (e.g. George VI Sound) within the Antarctic Peninsula forearc probably took place, related to the clockwise rotation of the angle of subduction from oblique to a more normal orientation. This change began at *c.* 62 Ma and drove a decline in subduction rates from over 10 to 4 cm a^{-1} by about 52 Ma (McCarron and Larter 1998). Evidence of dextral transtensional deformation can be seen within the Fossil Bluff Group on Alexander Island (Storey and Nell 1988).

The George VI Sound separates Alexander Island from Palmer Land of the Antarctic Peninsula and consists of a *c.* 600 km long 30–90 km wide channel some 2000 m deep, below sea-level. Seismic data and exposed bedrock show evidence of normal faulting consistent with an extensional tectonic setting (Crabtree *et al.* 1985; Doubleday and Storey 1998). Topographically, there are marked differences between the eastern margin of Alexander Island, where an escarpment rises sharply to *c.* 2500 m in the Douglas Range bounded by the LeMay Fault, and the lower relief of the western margin of Palmer Land, which rises from sea-level to an elevated (>1000 m) plateau some 150 km east of George VI Sound. In Palmer Land there are two major north–south-trending fault zones, inferred from radar and satellite images (Crabtree *et al.* 1985), the easternmost of which forms the boundary of the rift system and the western escarpment of Palmer Land (Maslanyj 1987) (Fig. 2). The LeMay Fault on Alexander Island defines the western boundary of the rift (Edwards 1980; Doubleday and Storey 1998).

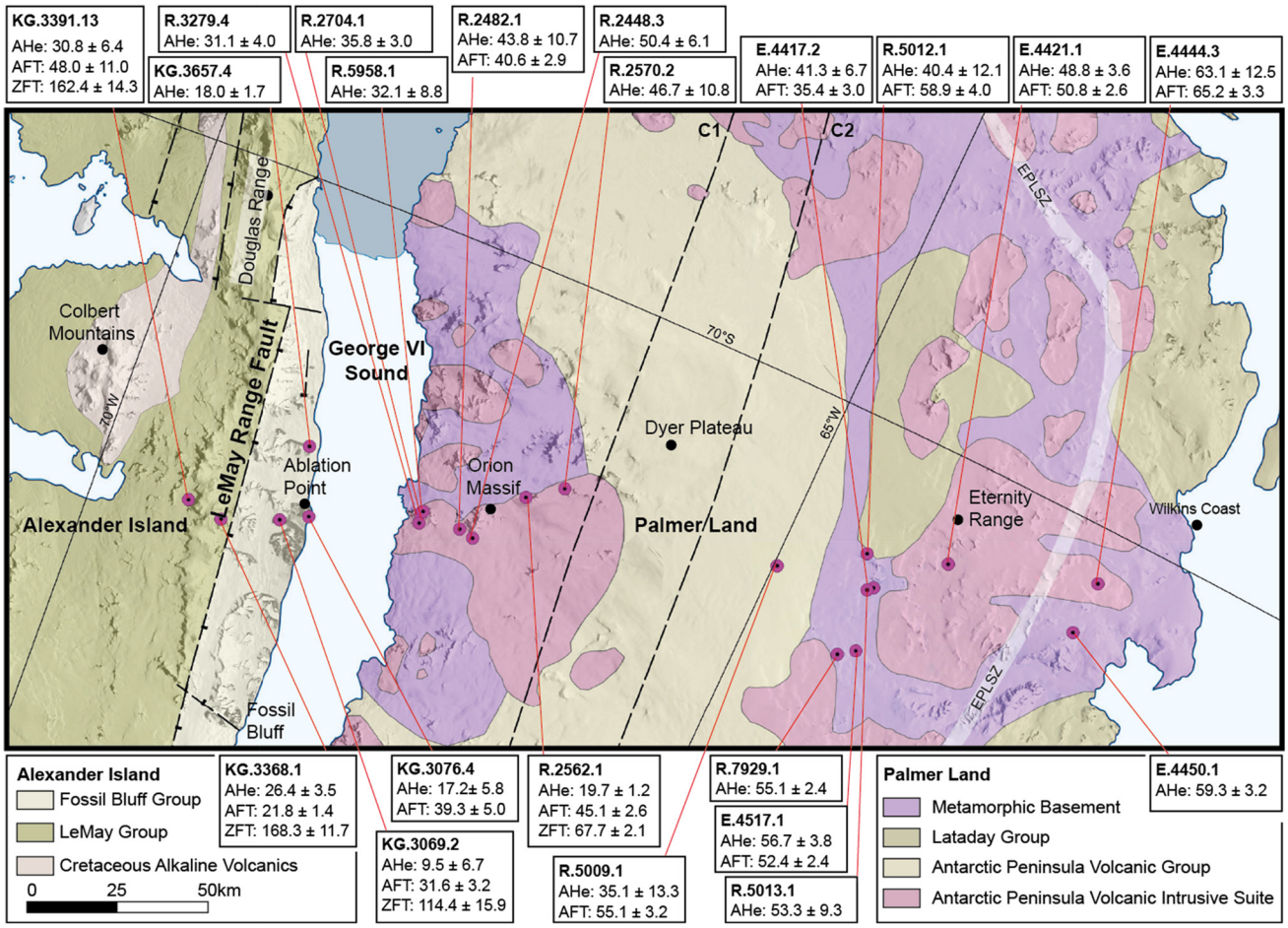

Fig. 3. Sample location and results for the transect across Alexander Island and Palmer Land. Fission-track (FT) errors are 1σ and standard deviation of replicates for the corrected mean AHe age. Inferred faults C1 and C2 are from Bell and King (1998). EPLSZ, Eastern Palmer Land Shear Zone (after Vaughan *et al.* 2002).

Methods

To define regional-scale spatial and temporal patterns in rock cooling histories 21 samples were collected as an east to west transect across the southern Antarctic Peninsula (Fig. 3). Samples were taken from the British Antarctic Survey rock archive spanning expeditions between 1973 and 2001. Samples from Alexander Island were from sedimentary rocks whereas Palmer Land samples comprised metamorphic and igneous lithologies. The sample transect is located in the region that represents the crustal segment where a ridge collision between the Heezen and Tula fracture zones took place between *c.* 40 and 25 Ma (Hole *et al.* 1994). Because of the extensive ice cover, there are no samples from easternmost Alexander Island. The partial retention zone (*c.* 80–40°C) of the (U–Th)/He (AHe) and partial annealing zone (*c.* 130–60°C) of the apatite fission-track (AFT) methods are well placed to provide constraints on timing, rate and magnitude of bedrock exhumation in the uppermost crust.

Thermochronometry analyses were performed at the London Geochronology Centre. Fission-track analyses were based on the external detector and zeta calibration approach (Hurford and Green 1983) with sample irradiations using the University of Munich FRM 11 thermal neutron facility at Garching, Germany. Apatites were mounted and etched in 5N nitric acid at 20°C for 20 s. Track length measurements were used to constrain sample cooling rate, and grain bulk composition was monitored using etch pit length (DPAR) measured parallel to the crystallographic *c*-axis (Donelick 1993). (U–Th)/He analyses included replicates. To reduce uncertainty associated with alpha ejection correction only whole, inclusion- and fracture-free apatite grains were selected. These were placed in platinum tubes and outgassed using a 25 W, 808 nm diode laser and ^{4}He measured on a Balzers quadrupole mass spectrometer. Following apatite dissolution and spiking, U, Th and Sm concentrations were measured on an Agilent 7900x inductively coupled plasma mass spectrometry system. Full details on the analytical protocols are provided in the Supplementary material.

The QTQt software (Gallagher 2012) based on a Bayesian trans-dimensional approach to data inversion was used to extract probable thermal histories. Input data included single-grain data and chemical characteristics. Model outputs are accepted thermal history models that can be combined to give a expected thermal history model, which is the mean of the accepted paths weighted by the posterior probability of each individual thermal history. This posterior distribution can also be used to define the 95% credible intervals that provide a measure of uncertainty. Model runs allowed the temperature offset to vary over time and data were predicted using the annealing and diffusion models of Ketcham *et al.* (2007) and Gautheron *et al.* (2009). In the absence of geological constraints, no initial boundary conditions were set, other than a present-day temperature of −10°C ± 10°C.

Results

AFT analyses were made on representative samples informed by the AHe results and sample location. Table 1 summarizes the AHe and AFT results. Full data and sample locations can be found in the Supplementary material (Table S1). AFT ages range from 21.8 ± 1.4 to 65.2 ± 3.3 Ma (Table S2). The central age for sample KG.3391.1

is based on only seven grain ages and hence is less reliable but it is included for comparison purposes as its age is similar to those of nearby samples. Most sample ages are between 35 ± 3 and 65 ± 3 Ma. Samples with reasonable numbers of measured track lengths (>75) have values between 13.8 μm (E.4421.1) and 14.4 μm (R2562.1), indicative of fast cooling followed by residence at low temperatures.

A total of 104 single-grain AHe dates were obtained from 20 samples. Numbers of replicates per sample varied according to apatite quality and yield. Single-grain dates range from 4.7 ± 0.4 to 78.6 ± 3.8 Ma (Table S3) and mean ages range from 9.5 ± 6.7 to 63.1 ± 3.0 Ma; however, seven of the 20 mean ages show wide dispersion of single-grain dates (greater than *c.* 20%). Wide data dispersion is likely, in most cases, to be real even for rapidly cooled samples although dispersion in single-grain dates, beyond that which can be accounted for by grain size and radiation damage (Flowers *et al.* 2009), may also be due to other factors such as composition (Djimbi *et al.* 2015), He implantation (Spiegel *et al.* 2009), fluid and mineral inclusions (Farley 2002; Vermeesch *et al.* 2007) and experimental issues such as incomplete grain dissolution and outgassing of He. As some of the overdispersion might be real we do not apply an arbitrary dispersion threshold or use statistical filtering methods as these have no real meaning. Instead, we adopted a cautious approach to data screening and confined the removal of grain ages to extreme outliers (e.g. Precambrian dates) and/or experimental criteria associated anomalous U/Th and He concentrations (full details are given in Table S3).

Table 1 summarizes sample locations with respect to distances from the trench and elevation. Ages generally increase towards the east (Fig. 4). The youngest ages occur in regions of lower elevations (<500 m) and most of the oldest ages are found across eastern Palmer Land at elevations >1000 m. AFT and AHe ages on Palmer Land overlap but across Alexander Island ages diverge, suggesting a different thermal history. Because collisions between the Antarctic–Phoenix ridge segments and the former trench along the Antarctic Peninsula would have transmitted stresses inland it is worth examining the data in relation to distance from the trench zone. This is shown in Figure 5. Two distinct trends are apparent, separated by the region that contains the easternmost shear zone of Crabtree *et al.* (1985), which marks the boundary of the George VI rift system, referred to as fault 2 (C2) by Bell and King (1998).

AFT and AHe ages across Palmer Land at elevations >1000 m are within error and fall between 35.4 ± 3.0 and 65.2 ± 3.3 Ma. This suggests that samples reached the uppermost crust (1–2 km) by the early Cenozoic and that since that time depths of erosion have remained low. This is supported by sample thermal history models (Fig. 6) that use both AFT and AHe data. Models show continuous cooling since the Late Cretaceous, reaching temperatures <60°C by 30 Ma. Samples E4443.3, E.4421.1 and E.4517.1 indicate a pulse of faster cooling from temperatures >120°C to <60°C between 70 and 55 Ma consistent with a period of accelerated exhumation. In contrast, thermal histories for westernmost Palmer Land and Alexander Island are more varied and record more recent cooling through the FT partial annealing and AHe partial retention zones. Samples from the fossil Bluff Group on Alexander Island, closest to George VI Sound at lowest elevations (from 70 to 180 m), record the youngest AHe ages, between 9 and 17 Ma, significantly younger than rocks at similar elevations on the eastern margin of George VI Sound, where AHe ages fall between 35 and 31 Ma. In summary, the thermal history models fall into two groups: Group 1 models, west of the C2 fault on Palmer Land, record cooling to shallow crustal levels (<60°C) between *c.* 70 and 50 Ma; Group 2 models, west of the C2 faults, including Alexander Island, are dominated by more recent cooling to shallow crustal levels (<60°C) *c.* 25–15 Ma, although some models also show evidence for the earlier phase of cooling in Group 1.

Interpolating QTQt outputs

Figure 6 is a simplified summary of the QTQt models that omits uncertainties and makes a qualitative interpretation of their spatial significance. A better approach is to synthesize the results of QTQt and visualize cooling rates that vary in space and time, and present cooling as a function of distance from the trench and time. This requires interpolating our cooling rates into this space and averaging rates from different samples. A simple approach would be to take the cooling rates returned by the expected model, which vary as a function of space and time, and interpolate a surface between these

Table 1. *Summary of mean AFT and AHe ages for samples in Figures 4 and 5.*

Sample	Lithology	Elevation (m a.s.l.)	Trench (km)	AFT central age (Ma)	ZFT central age (Ma)	AHe mean age (Ma)
KG.3391.13	Siltstone	940	393	48.0 ± 11.0*	162.4 ± 14.3*	29.9 ± 2.0
KG.3368.1	Sandstone	1200	402	21.8 ± 1.4	168.3 ± 11.7*	27.7 ± 1.9
KG.3657.4	Sandstone	180	394			18.0 ± 1.7
KG.3069.2	Conglomerate	440	412	34.2 ± 5.7	114.4 ± 15.9*	9.5 ± 6.7
KG.3076.4	Sandstone	70	407	52.3 ± 9.3		17.2 ± 5.8
R.2704.1	Diorite	180	428			35.8 ± 3.0
R.5958.1	Diorite	180	421			32.1 ± 8.8
R.3279.4	Diorite	150	432			31.1 ± 4.0
R.2482.1	Diorite	340	425	40.6 ± 2.9		43.8 ± 10.7
R.2562.1	Gneiss	870	428	45.1 ± 2.6	67.7 ± 2.1	19.7 ± 1.2
R.2570.2	Granodiorite	910	435			46.7 ± 10.8
R.5009.1	Granite	900	478	55.1 ± 3.2		35.1 ± 13.3
R.5012.1	Diorite	1890	488	58.9 ± 4.0		40.4 ± 12.1
R.5013.1	Diorite	1430	500			53.3 ± 9.3
R.7929.1	Granite	1540	530			55.1 ± 2.4
E.4417.2	Gneiss	1620	521	35.4 ± 3.0		41.3 ± 6.7
E.4517.1	Schist	1460	510	52.4 ± 2.4		56.7 ± 3.8
E.4421.1	Granite	1500	503	50.8 ± 2.6		48.8 ± 3.6
E.4444.3	Diorite	1010	550	65.2 ± 3.3		63.1 ± 12.5
E.4450.1	Gneiss	820	542			59.3 ± 3.2

a.s.l., above sea-level; ZFT, zircon fission-track. Mean AHe ages are corrected for alpha ejection and report the standard deviation. Elevation and distance from trench are from Fretwell *et al.* (2013).
*From Storey *et al.* (1996*a*).

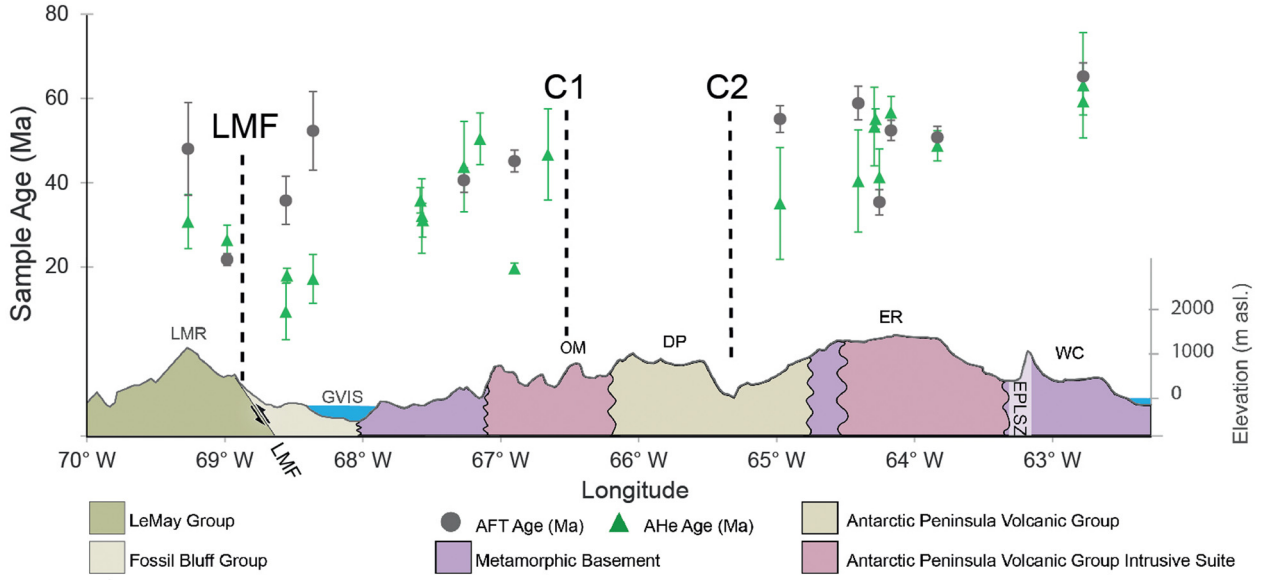

Fig. 4. Mean AFT and AHe ages plotted against sample location. Grey circles, AFT ages (Ma); green triangles, AHe ages (Ma); error bars are 1σ (AFT) and sample standard deviation (AHe). Elevation data are from Fretwell *et al.* (2013). LMR, LeMay Range; LMF, LeMay Range Fault; GVIS, George VI Sound; OM, Orion Massif; DP, Dyer Plateau; ER, Eternity Range; EPLSZ, Eastern Palmer Land Shear Zone; WC, Wilkins Coast.

points. However, this requires differentiating potentially noisy thermal histories, where noise is the result of averaging cooling histories made up of linear segments with abrupt changes in cooling rates. We would also have to specify additional parameters designed to control the smoothness of this interpolation and prevent extrapolation. To circumnavigate the requirement to calculate noisy cooling rates, we can work directly with temperatures. In this way, the output of QTQt represents likely temperatures, and uncertainties, at different times. In turn, we can state that a single temperature at a specific time in an expected thermal history is equal to the cooling rate history through time from the present day to that specific time,

$$T = T_s + \int_0^t \dot{c}\,\mathrm{d}t'$$

where T is temperature, T_s is the surface temperature, $\dot{c}$ is the cooling rate, t is time and t' is a dummy variable for integration. Next, we discretize distance from the trench into pixels of size Δx, so that

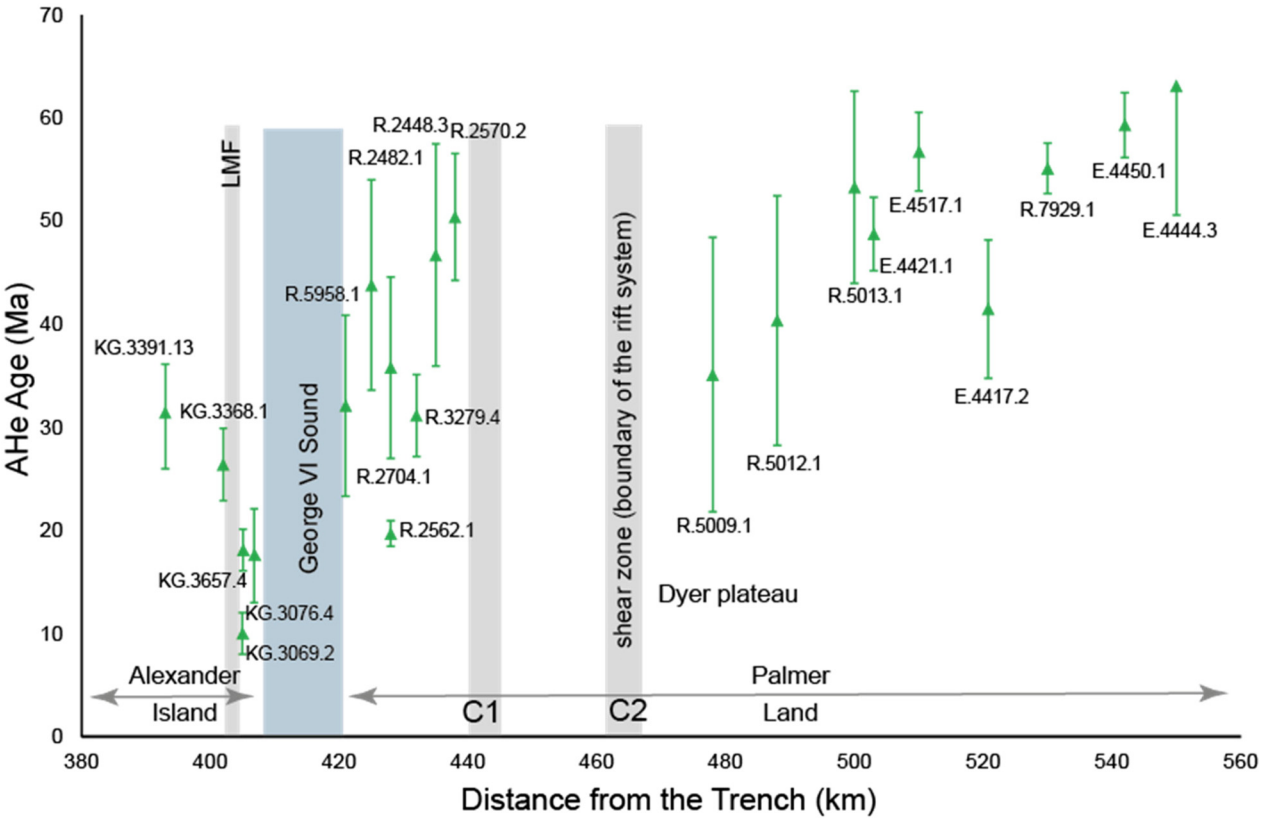

Fig. 5. Plot of mean AHe age v. distance from trench at present time using data from Fretwell *et al.* (2013). Error bars are the standard deviation of sample replicate ages. C1 and C2 are the locations of two major fault zones described by Crabtree *et al.* (1985) and Bell and King (1998).

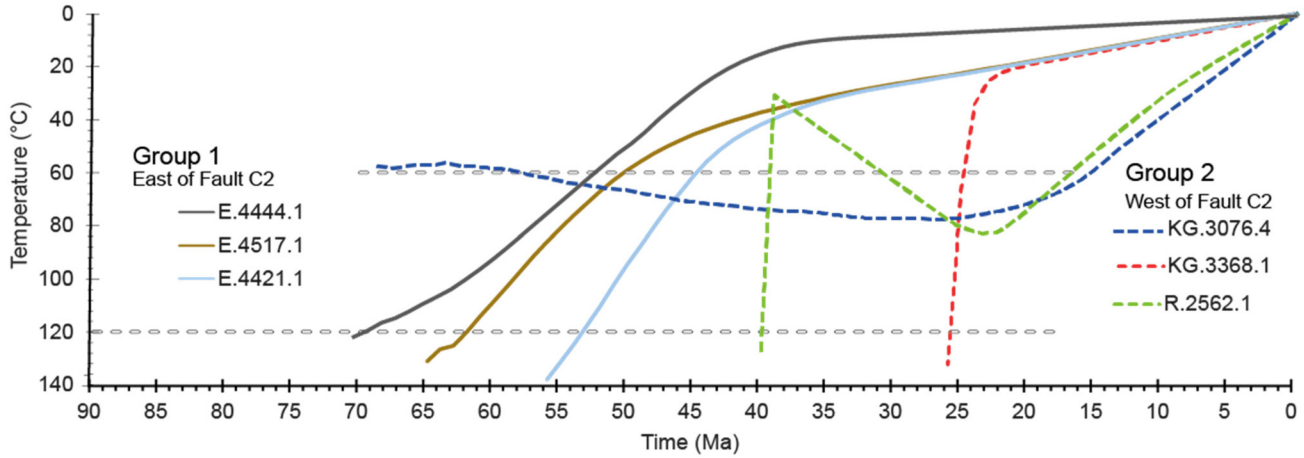

Fig. 6. Representative best-fit QTQt thermal history models showing contrasting thermal histories on either side of the eastern boundary fault (C2) on Palmer Land. Details of models are provided in Supplementary material Fig. S1.

within each increment of Δx the thermal history is constant. We discretize the time resolved by the thermochronometric data into time steps Δt. This provides pixels of size Δx by Δt within which the cooling history is constant. Therefore, a sample's location determines which spatial pixels it resolves, and the temporal pixels are defined by the length of the thermal history. For example, a sample that is a specific distance from the trench may belong to the ith spatial pixel and a specific point along the thermal history may belong to the mth temporal pixel. Therefore, we could write the integral above as a summation of cooling rates multiplied by time steps through m pixels:

$$T_{i,m} = T_s + \sum_{j=1}^{m} \dot{c}_{i,j} \Delta t.$$

This can be rewritten as a vector product, with a vector of time steps that sum to the time the temperature corresponds to the vector of cooling rates. This can be combined with similar expressions for different points on the same thermal history and points of thermal histories from other locations in a matrix vector product:

$$\boldsymbol{G}\boldsymbol{c} = \boldsymbol{T}$$

where $\boldsymbol{G}$ is a matrix containing time steps, $\boldsymbol{c}$ is a vector of cooling rates and $\boldsymbol{T}$ is a vector of temperatures. To solve this equation and also estimate cooling rates in spatial locations where we do not have data or at times where we have no resolution, we add the constraint that cooling rates vary smoothly in space. We do this by adding a system of equations that require that the negative Laplacian of the cooling rates between neighbouring locations is close to zero. We also detrend the temperature data by removing an expected cooling rate of 5°C Ma^{-1} from the temperatures. In the absence of any effective data, the cooling rate will revert to this expected cooling rate. Therefore, we have the following matrix-vector product:

$$\begin{pmatrix} \boldsymbol{W}_d G \\ \alpha \boldsymbol{W} \end{pmatrix} (c - \boldsymbol{c}_e) = \begin{pmatrix} \boldsymbol{W}_d T - G\boldsymbol{c}_e \\ 0 \end{pmatrix}$$

where $\boldsymbol{W}_d$ is a weighting matrix of temperatures where individual entries correspond to specific temperature points and are given by one over the temperature uncertainty, $\alpha \boldsymbol{W}$ is a weighting matrix for cooling histories that penalizes models that are not smooth in space and $\boldsymbol{c}_e$ is a vector containing the expected cooling rates. $\boldsymbol{W}$ is calculated based on the Laplacian of the cooling rates in space: if there are no spatial curvatures in cooling rate (e.g. rates are constant in space), the Laplacian will be equal to zero and the lower half of the above equation will be satisfied. Δx is set to 2 km and Δt is set to 5 km. We solve for the cooling values in space and time using bounded iterative methods, with rates free to vary between −5 and 15°C Ma^{-1}. A value of unity is used for α and this resulted in maps that are relatively smooth but still capture the cooling patterns that can be identified by inspecting the individual cooling histories for each sample.

To propagate temperature uncertainty to uncertainty on rates of cooling, we resample the residuals. To do this, we randomly perturb the observed temperatures by a random residual between the observed and predicted temperature estimates. This results in a new, modified, temperature dataset that we can use in the inversion and predict cooling rates. The process is repeated 1000 times, resulting in an ensemble of cooling rates for each point in the distance to trench–time space. The cooling rates at each pixel are then ranked and the central 68% of the models is used to define the uncertainty. This form of bootstrapping provides an indication of the uncertainty of cooling rates for visualization purposes; however, for uncertainties associated with specific thermal histories, it is essential to assess the output from QTQt (Fox and Carter 2020).

Figure 7 shows the results of transforming the QTQt models to a single plot of cooling as a function of distance from the trench and time. Figure 7b defines three areas of faster cooling, each bounded by structural features; the fastest cooling rates are recorded west of the LeMay Fault. The most recent cooling occurs within the George VI Sound Rift and the oldest fast cooling rates occur furthest from the trench zone beyond rift-related structures. We can also see that where we have samples at a specific distance from the trench, uncertainty on the cooling rates is small (Fig. 7b). Where there are no data, uncertainties are larger. Uncertainties are larger closer to the present where the temperatures are forced to reach surface temperatures. By bootstrapping the residuals, a large temperature residual may perturb a recent temperature to a large degree. Because samples are forced to reach surface temperatures, this may result in rapid cooling or even reheating. In contrast, at points further back in time cooling rates in other time intervals can compensate for anomalous cooling rates.

Discussion

The significance of spatio-temporal patterns of rock cooling and exhumation recorded by the apatite thermochronometry results (Fig. 7) are considered in the context of the evolving ridge subduction setting, coupling between the ridge and the overriding plate, causes and timing of extension and crustal heating and uplift from upwelling asthenosphere through a slab window. Similar to most subduction zones, Cenozoic subduction along the Antarctic Peninsula was oblique and this resulted in strain partitioning within

the forearc region accompanied by strike-slip motion along one or more faults within the overriding plate, parallel to the trench. Obliquity also means that along-strike subduction velocities would have varied and led to the gradual rotation of the lower and upper plates, creating both compression and extension (McCaffrey 1992; Chemenda *et al.* 2000). Doubleday and Storey (1998) noted that dextral transtensional structures on Alexander Island formed when the forearc was in extension and that sinistral transpressional structures in the LeMay Group sequences are related to a compressional forearc setting from the Middle Jurassic to the Early Cretaceous. This kinematic regime is also evident along the wide Gondwana margin. Vaughan *et al.* (2012) correlated this pre-100 Ma compressional event to Phase 1 of the Palmer Land tectonic event.

The extension is controlled by toroidal mantle flow along slab edges, or lateral mantle flow owing to oblique subduction geometry (Balázs *et al.* 2021), and the extensional stresses would have been transferred hundreds of kilometres from the trench into the overriding plate, exploiting any inherited, thermal (arc) or rheologically weak zones. In this context, the most notable structural features across the study region relate to the George VI Sound, which is bounded to the west by the north–south LeMay Range Fault. This is a strike-slip fault that underwent major movement in the Middle Jurassic and exhibits later dextral strike-

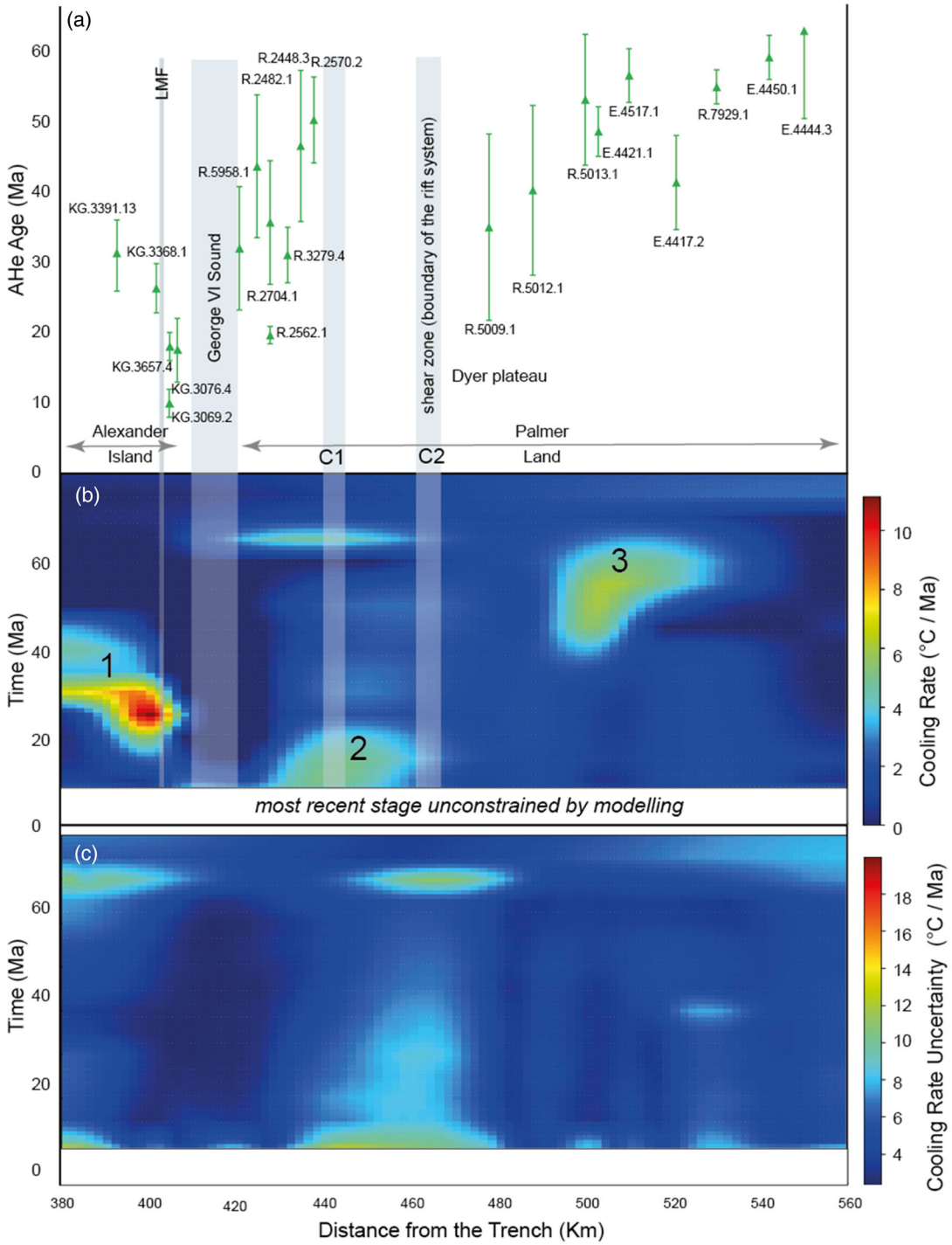

Fig. 7. (**a**) Comparison of ages with respect to major structures and distance from the trench. (**b**) Results of transforming the QTQt models to a single plot that shows how cooling rates vary across the study area. Three intervals of accelerated cooling are recognized, labelled 1–3. (**c**) Uncertainties of model rates of cooling.

slip fault motion, probably owing to the oblique subduction of the Phoenix Plate (Storey and Nell 1988). Seismic data have imaged a low-angle detachment beneath George VI Sound, consistent with a major tectonic feature (Bell and King 1998). To the east of George VI Sound two major north–south-trending fault zones define the western escarpment of Palmer Land (Crabtree *et al.* 1985; Bell and King 1998) and serve as the structural boundary of the George VI rift system. Storey *et al.* (1996*b*) proposed that dextral transtensional deformation observed in the region of George VI Sound (Storey and Nell 1988) resulted from an Eocene decrease in convergence rate. Marine magnetic data for the Early Paleocene show that around 62–63 Ma (chron C27) convergence offshore Alexander Island changed, with a *c.* 30° clockwise rotation that led to a decline in spreading rates. Bell and King (1998) considered that the most likely age for subduction-related rifting was between 50 and 30 Ma when subduction rates decreased.

Reconstructions of the former positions of the trench show that the greatest amount of rollback along the peninsula was centred on Alexander Island and that most of this occurred between 90 and 65 Ma (McCarron and Larter 1998). This time interval broadly corresponds to the early cooling seen in 1 in Figure 7b. Late Cretaceous subduction along the West Antarctic margin, including the Antarctic Peninsula, probably involved part of the Bellingshausen Plate (Cande and Kent 1995) although by 62 Ma it was extinct (Eagles *et al.* 2004). The convergence history of the Phoenix Plate is better constrained and plate reconstructions show that between chrons C34 and C32 (83–68 Ma), spreading was fast and that convergence of the Phoenix Plate offshore Alexander Island was high, around 10–12 cm a^{-1}. By *c.* 62–63 Ma (chron 27) the Phoenix Plate changed direction to the SE and this reduced convergence rates. By 52 Ma rates had dropped by over half (McCarron and Larter 1998). It is these changes that probably explain the early phase of accelerated cooling recorded by 1 in Figure 7b.

Thermal history models, from eastern Palmer Land (samples E4443.3, E.4421.1 and E.4517.1), show either well-resolved accelerated cooling between 80 and 55 Ma followed by uninterrupted slower cooling to the present, or uninterrupted slow cooling (R.5009.1, R5012.1) (Fig. 6). The rapid and then slow cooling could be due to changes in exhumation rate under a constant and a linear geothermal gradient, but because the zircon FT to AFT ages (R2562.1) require rapid cooling across at least 100°C it is more likely that it represents a period of rock uplift and erosion that elevates the geothermal gradient owing to the advection of heat. Once exhumation rates decrease, the geothermal gradients relax but rocks continue to be exhumed to give uninterrupted slower cooling to the present. In this scenario peak cooling rates would post-date the onset of active rock uplift. Such an interpretation would fit with high rates of strain and deformation associated with a regime of fast rates of plate spreading. We therefore favour a period of regional Late Cretaceous–Paleocene uplift driven by high rates of convergence to explain the early cooling (1) in Figure 7b from eastern Palmer Land. This timing postdates the two-phase mid-Cretaceous Palmer Land deformation events (Vaughan *et al.* 2012) and changes in the rate of opening of the southern Weddell Sea (König and Jokat 2006). Riley *et al.* (2020) investigated Late Cretaceous–Paleocene volcanism of the Dyer Plateau region and identified peaks in magmatism at 108, 93 and 64 Ma, with a locus *c.* 120 km from the trench. They demonstrated that convergence rates between the Phoenix Plate and the Antarctic Peninsula were elevated (>20 cm a^{-1} between 135 and 100 Ma, with a significant decrease in convergence rates (<10 cm a^{-1}) by *c.* 95 Ma. The higher rates of convergence overlap with the emplacement of the Lassiter Coast intrusive suite (Riley *et al.* 2018).

The second group of apatite thermal histories in Figure 6 (represented by accelerated cooling groups 2 and 3 in Fig. 7b) are from samples spanning westernmost Palmer Land and Alexander Island. These record a more varied and recent cooling history that includes asymmetric mean ages between the eastern and western coastal margins of George VI Sound with AHe ages between 9 and 17 Ma on Alexander Island and between 35 and 31 Ma on the conjugate Palmer Land side. On Alexander Island AFT ages are similar, between 35.7 ± 5.7 and 27.7 ± 1.5 Ma, but the mean AHe ages are younger (<18 Ma compared with ≥30 Ma) west of the Le May Range Fault (Fig. 5). In part, these differences relate to topography whereby western samples are from elevations around 940–1200 m in contrast to 70–180 m for the younger ages bordering the George VI Sound. Thermal history models of Group 2 samples (Fig. 6) include two samples that show a period of reheating prior to cooling between *c.* 25 and 15 Ma. The same timing is evident on both sides of the George VI Sound (Fig. 7b) but is not present in Palmer Land east of the C2 fault. The thermal history for sample KG.3368.1 (elevation 940 m), closest to the Le May Range Fault, shows a clear signal of rapid cooling at 25 Ma. These relationships imply that the rift zone was affected by deformation and rock uplift that began at *c.* 25 Ma, and that this involved the Le May Range Fault. Oligocene reheating seen in R2562.1 and KG3076.4 (Fig. 6) might be related to a small amount of subsidence of the overriding plate in the arc and back-arc area contemporaneous with uplift of the forearc region as predicted by analogue modelling (Martinod *et al.* 2013). However, further sampling would be needed to better constrain this event.

The LeMay Range Fault has a long history that extends back to the Jurassic. Three phases of deformation have been recognized (Doubleday and Storey 1998), the most recent of which involved dextral strike-slip fault motion as seen in the Fossil Bluff Group sediments that were uplifted and deformed under a dextral transpressive regime. Nell and Storey (1991) ascribed this to the oblique subduction between the Heezen and Tharp fracture zones between 50 and 30 Ma, but the cooling recorded by the apatite thermal history models is marginally younger and better fits with the cessation of subduction owing to trench collision of a ridge segment NE of the Heezen fracture zone, offshore northern Alexander Island, dated to *c.* 30 ± 3 Ma (Larter and Barker 1991; Hole *et al.* 1994).

Finally, we consider the potential role of a slab window below the study area. Subduction-related magmatism on Alexander Island includes low-Ca, high-Mg andesite magmas diagnostic of anomalously hot forearc regions (Hole *et al.* 1994; McCarron and Smellie 1998). These have been linked to the development of a slab window that now extends for more than 2000 km under the length of the peninsula. Models for Antarctic Peninsula slab window formation show a progressive unzipping, from south to north, following the northeastward younging of ridge crest–trench collisions (Hole *et al.* 1994). For Alexander Island, slab window formation would have taken place after subduction ceased between *c.* 50 Ma in the south and after 30 Ma in the north, when the ridge segment NE of the Heezen fracture zone reached the margin (Larter and Barker 1991). The Paleogene Farallon Plate–Phoenix Ridge collision in Patagonia also led to the development of a major slab window and extension was associated with high-Mg, high-Ti magmatism (Aragón *et al.* 2013).

Slab windows affect the thermal and mechanical structure of the overlying lithosphere, increasing temperatures in the forearc (Groome and Thorkelson 2009) and driving transient isostatic uplift (Guenthner *et al.* 2010; Braun *et al.* 2013), as seen, for example, by the isostatic uplift of the Alaskan forearc and arc (Kortyna *et al.* 2013). Thermal effects from the slab window are unlikely to be detected on Alexander Island owing to its distance from the trench and the dissipation of heat over time (Groome and Thorkelson 2009). More importantly, results from this study show spatial variations in apatite cooling histories that are inconsistent with regional signatures expected from heating by a slab window. In

Patagonia, where Miocene collision of the Chile Ridge formed a slab window, a thermochronological study also found no evidence for slab window heating (Stevens Goddard and Fosdick 2019).

Slab window isostatic uplift could produce apatite cooling ages that track a migrating wave of uplift and erosion that progressed eastwards from the trench side to the west, to produce a systematic eastward younging of exhumation. Our dataset shows no single systematic trend although there is a tendency for ages to increase to the east, which is opposite to that expected from a slab window (Fig. 5). Stevens Goddard and Fosdick (2019) observed a latitudinal control on regional rock uplift and erosion in the southern Patagonian Andes but linked this to a migrating thickened crustal welt along the leading edge of a subducting ridge rather than directly to the slab window. This may be the case for the Antarctic Peninsula (e.g. the trend observed by Guenthner *et al.* 2010) but additional data from north of Alexander Island would be needed to test this.

Conclusions

Our apatite thermochronometry data and thermal history models have identified two well-defined periods of accelerated cooling that affected different parts of the southern Antarctic Peninsula. Results are interpreted in the context of regional deformation associated with the kinematics of subduction. The earliest cooling event is detected in eastern Palmer Land and dates to the end of the Cretaceous when convergence rates of the Phoenix Plate offshore Alexander Island fell by over half from 12 to <5 cm a^{-1} as the direction of convergence moved to the SE. The younger event began *c.* 25 Ma and affected Western Palmer Land and Alexander Island. This younger phase of accelerated cooling is confined within the boundary of a rift system that includes the George VI Sound. The cause is probably related to trench collision of a ridge segment NE of the Heezen fracture zone. Finally the results were considered in relation to the development of a slab window that progressively unzipped, from south to north, following the northeastward younging of ridge crest–trench collisions. Slab windows are expected to produce apatite cooling ages that track a migrating wave of uplift and erosion and show a systematic eastward younging of exhumation. No such trend is observed and thus a direct influence from a slab window is discounted for the southern Antarctic Peninsula.

Acknowledgements The rock samples this paper is based on were kindly supplied by M. Evans from the British Antarctic Survey Rock Repository. We thank the Editor and C. Marks for their thoughtful comments, which have improved the quality of this paper.

Author contributions **GT**: conceptualization (lead), formal analysis (lead), investigation (lead), writing – original draft (equal); **TR**: writing – original draft (supporting); **MF**: formal analysis (supporting), visualization (supporting), writing – original draft (supporting); **AC**: conceptualization (supporting), formal analysis (supporting), writing – original draft (equal)

Funding This research received no specific grant from any funding agency in the public, commercial or not-for-profit sectors.

Competing interests The authors declare that they have no known competing financial interests or personal relationships that could have appeared to influence the work reported in this paper.

Data availability Datasets for this research are provided in Supporting Information Tables S1 to S3. Data are also available at Pangaea https://doi.pangaea.de/10.1594/PANGAEA.942483

Scientific editing by Darren Mark and Graham Shields

References

Anderson, J.B., Warny, S. *et al.* 2011. Progressive Cenozoic cooling and the demise of Antarctica's last refugium. *Proceedings of the National Academy of Sciences of the USA*, **108**, 11356–11360, https://doi.org/10.1073/pnas.1014885108

Aragón, E., Pinotti, L. *et al.* 2013. The Farallon–Aluk ridge collision with South America: implications for the geochemical changes of slab window magmas from fore- to back-arc. *Geoscience Frontiers*, **4**, 377–388, https://doi.org/10.1016/j.gsf.2012.12.004

Balázs, A., Faccenna, C., Ueda, K., Funiciello, F., Boutoux, A., Blanc, E.J. and Gerya, T. 2021. Oblique subduction and mantle flow control on upper plate deformation: 3D geodynamic modeling. *Earth and Planetary Science Letters*, **569**, 117056, https://doi.org/10.1016/j.epsl.2021.117056

Barker, P. 1982. The Cenozoic subduction history of the Pacific margin of the Antarctic Peninsula: ridge crest–trench interactions. *Journal of the Geological Society, London*, **139**, 787–801, https://doi.org/10.1144/gsjgs.139.6.0787

Bell, A.C. and King, E.C. 1998. New seismic data support Cenozoic rifting in George VI Sound, Antarctic Peninsula. *Geophysical Journal International*, **134**, 889–902, https://doi.org/10.1046/j.1365-246x.1998.00605.x

Braun, J., Robert, X. and Simon-Labric, T. 2013. Eroding dynamic topography. *Geophysical Research Letters*, **40**, 1494–1499, https://doi.org/10.1002/grl.50310

Burton-Johnson, A. and Riley, T.R. 2015. Autochthonous v. accreted terrane development of continental margins: a revised *in situ* tectonic history of the Antarctic Peninsula. *Journal of the Geological Society, London*, **172**, 822–835, https://doi.org/10.1144/jgs2014-110

Butterworth, P.J., Crame, J.A., Howlett, P.J. and Macdonald, D.I.M. 1988. Lithostratigraphy of Upper Jurassic–Lower Cretaceous strata of eastern Alexander Island, Antarctica. *Cretaceous Research*, **9**, 249–264, https://doi.org/10.1016/0195-6671(88)90020-1

Cande, S.C. and Kent, D.V. 1995. Revised calibration of the geomagnetic polarity timescale for the Late Cretaceous and Cenozoic. *Journal of Geophysical Research: Solid Earth*, **100**, 6093–6095, https://doi.org/10.1029/94JB03098

Castillo, P., Lacassie, J.P., Augustsson, C. and Herve, F. 2015. Petrography and geochemistry of the Carboniferous–Triassic Trinity Peninsula Group, West Antarctica: implications for provenance and tectonic setting. *Geological Magazine*, **152**, 575–588, https://doi.org/10.1017/S0016756814000454

Chemenda, A., Lallemand, S. and Bokun, A. 2000. Strain partitioning and interplate friction in oblique subduction zones: constraints provided by experimental modeling. *Journal of Geophysical Research: Solid Earth*, **105**, 5567–5581, https://doi.org/10.1029/1999JB900332

Clinger, A.E., Fox, M., Balco, G., Cuffey, K. and Shuster, D.L. 2020. Detrital thermochronometry reveals that the topography along the Antarctic Peninsula is not a Pleistocene landscape. *Journal of Geophysical Research: Earth Surface*, **125**, e2019JF005447, https://doi.org/10.1029/2019JF005447

Constantino, R.R., Tinto, K.J., Bell, R.E., Porter, D.F. and Jordan, T.A. 2020. Seafloor depth of George VI Sound, Antarctic Peninsula, from inversion of aerogravity data. *Geophysical Research Letters*, **47**, e2020GL088654, https://doi.org/10.1029/2020GL088654

Crabtree, R.D., Storey, B.C. and Doake, C.S.M. 1985. The structural evolution of George VI Sound, Antarctic Peninsula. *Tectonophysics*, **114**, 431–442, https://doi.org/10.1016/0040-1951(85)90025-3

Crame, J., Pirrie, D. and Riding, J.B. 2006. Mid-Cretaceous stratigraphy of the James Ross Basin, Antarctica. *Geological Society, London, Special Publications*, **258**, 7–19, https://doi.org/10.1144/GSL.SP.2006.258.01.02

Djimbi, D.M., Gautheron, C., Roques, J.M., Tassan-Got, L., Gerin, C. and Simoni, E. 2015. Impact of apatite chemical composition on (U–Th)/He thermochronometry: an atomistic point of view. *Geochimica et Cosmochimica Acta*, **167**, 162–176, https://doi.org/10.1016/j.gca.2015.06.017

Donelick, R. 1993. Apatite etching characteristics versus chemical composition. *Nuclear Tracks and Radiation Measurements*, **21**, 604, https://doi.org/10.1016/1359-0189(93)90241-Z

Doubleday, P., Macdonald, D. and Nell, P. 1993. Sedimentology and structure of the trench-slope to forearc basin transition in the Mesozoic of Alexander Island, Antarctica. *Geological Magazine*, **130**, 737–754, https://doi.org/10.1017/S0016756800023128

Doubleday, P.A. and Storey, B.C. 1998. Deformation history of a Mesozoic forearc basin sequence on Alexander Island, Antarctic Peninsula. *Journal of South American Earth Sciences*, **11**, 1–21, https://doi.org/10.1016/S0895-9811(97)00032-1

Eagles, G., Gohl, K. and Larter, R.D. 2004. Life of the Bellingshausen plate. *Geophysical Research Letters*, **31**, L07603, https://doi.org/10.1029/2003GL019127

Eagles, G., Larter, R.D., Gohl, K. and Vaughan, A.P.M. 2009. West Antarctic rift system in the Antarctic Peninsula. *Geophysical Research Letters*, **36**, L21305, https://doi.org/10.1029/2009gl040721

Edwards, C. 1980. New evidence of major faulting on Alexander Island. *British Antarctic Survey Bulletin*, **49**, 15–20.

Farley, K.A. 2002. (U–Th)/He dating: techniques, calibrations, and applications. *Reviews in Mineralogy and Geochemistry*, **47**, 819–844, https://doi.org/10.2138/rmg.2002.47.18

Flowers, R.M., Ketcham, R.A., Shuster, D.L. and Farley, K.A. 2009. Apatite (U–Th)/He thermochronometry using a radiation damage accumulation and annealing model. *Geochimica et Cosmochimica Acta*, **73**, 2347–2365, https://doi.org/10.1016/j.gca.2009.01.015

Fox, M. and Carter, A. 2020. Heated topics in thermochronology and paths towards resolution. *Geosciences*, **10**, 375, https://doi.org/10.3390/geosciences10090375

Fretwell, P., Pritchard, H.D. *et al.* 2013. Bedmap2: improved ice bed, surface and thickness datasets for Antarctica. *Cryosphere*, **7**, 375–393, https://doi.org/10.5194/tc-7-375-2013

Gallagher, K. 2012. Transdimensional inverse thermal history modeling for quantitative thermochronology. *Journal of Geophysical Research: Solid Earth*, **117**, https://doi.org/10.1029/2011JB008825

Gautheron, C., Tassan-Got, L., Barbarand, J. and Pagel, M. 2009. Effect of alpha-damage annealing on apatite (U–Th)/He thermochronology. *Chemical Geology*, **266**, 157–170, https://doi.org/10.1016/j.chemgeo.2009.06.001

Groome, W.G. and Thorkelson, D.J. 2009. The three-dimensional thermo-mechanical signature of ridge subduction and slab window migration. *Tectonophysics*, **464**, 70–83, https://doi.org/10.1016/j.tecto.2008.07.003

Guenthner, W.R., Barbeau, D.L., Reiners, P.W. and Thomson, S.N. 2010. Slab window migration and terrane accretion preserved by low-temperature thermochronology of a magmatic arc, northern Antarctic Peninsula. *Geochemistry, Geophysics, Geosystems*, **11**, Q03001, https://doi.org/10.1029/2009GC002765

Hole, M., Saunders, A., Rogers, G. and Sykes, M. 1994. The relationship between alkaline magmatism, lithospheric extension and slab window formation along continental destructive plate margins. *Geological Society, London, Special Publications*, **81**, 265–285, https://doi.org/10.1144/GSL.SP.1994.081.01.15

Hole, M.J. 1988. Post-subduction alkaline volcanism along the Antarctic Peninsula. *Journal of the Geological Society, London*, **145**, 985–998, https://doi.org/10.1144/gsjgs.145.6.0985

Hunter, M., Riley, T., Cantrill, D., Flowerdew, M. and Millar, I. 2006. A new stratigraphy for the Latady Basin, Antarctic Peninsula: part 1, Ellsworth Land Volcanic Group. *Geological Magazine*, **143**, 777–796, https://doi.org/10.1017/S0016756806002597

Hunter, M.A. and Cantrill, D.J. 2006. A new stratigraphy for the Latady Basin, Antarctic Peninsula: part 2, Latady Group and basin evolution. *Geological Magazine*, **143**, 797–819, https://doi.org/10.1017/S0016756806002603

Hurford, A.J. and Green, P.F. 1983. The zeta age calibration of fission-track dating. *Chemical Geology*, **41**, 285–317, https://doi.org/10.1016/S0009-2541(83)80026-6

Ketcham, R.A., Carter, A., Donelick, R.A., Barbarand, J. and Hurford, A.J. 2007. Improved modeling of fission-track annealing in apatite. *American Mineralogist*, **92**, 799–810, https://doi.org/10.2138/am.2007.2281

König, M. and Jokat, W. 2006. The Mesozoic breakup of the Weddell Sea. *Journal of Geophysical Research: Solid Earth*, **111**, https://doi.org/10.1029/2005JB004035

Kortyna, C., Donaghy, E., Trop, J. and Idleman, B. 2013. Integrated provenance record of a forearc basin modified by slab-window magmatism: detrital-zircon geochronology and sandstone compositions of the Paleogene Arkose Ridge Formation, south–central Alaska. *Basin Research*, **26**, 436–460, https://doi.org/10.1111/bre.12033

Lallemand, S., Heuret, A. and Boutelier, D. 2005. On the relationships between slab dip, back-arc stress, upper plate absolute motion, and crustal nature in subduction zones. *Geochemistry, Geophysics, Geosystems*, **6**, Q09006, https://doi.org/10.1029/2005GC000917

Larter, R.D. and Barker, P.F. 1991. Effects of ridge crest–trench interaction on Antarctic–Phoenix spreading: forces on a young subducting plate. *Journal of Geophysical Research: Solid Earth*, **96**, 19583–19607, https://doi.org/10.1029/91JB02053

Larter, R., Rebesco, M., Vanneste, L., Gamboa, L. and Barker, P. 1997. Cenozoic tectonic, sedimentary and glacial history of the continental shelf west of Graham Land, Antarctic Peninsula. *In:* Barker, P.F. and Cooper, A.K. (eds) *Geology and Seismic Stratigraphy of the Antarctic Margin 2, Antarctic Research Series*. American Geophysical Union, Washington, D.C., **71**, 1–27, https://doi.org/10.1029/AR071p0001

Leat, P.T., Scarrow, J.H. and Millar, I.L. 1995. On the Antarctic Peninsula batholith. *Geological Magazine*, **132**, 399–412, https://doi.org/10.1017/S0016756800021464

Martinod, J., Guillaume, B., Espurt, N., Faccenna, C., Funiciello, F. and Regard, V. 2013. Effect of aseismic ridge subduction on slab geometry and overriding plate deformation: insights from analogue modeling. *Tectonophysics*, **588**, 39–55, https://doi.org/10.1016/j.tecto.2012.12.010

Maslanyj, M. 1987. Seismic bedrock depth measurements and the origin of George VI Sound, Antarctic Peninsula. *British Antarctic Survey Bulletin*, **75**, 51–65.

McCaffrey, R. 1992. Oblique plate convergence, slip vectors, and forearc deformation. *Journal of Geophysical Research: Solid Earth*, **97**, 8905–8915, https://doi.org/10.1029/92JB00483

McCarron, J.J. and Larter, R.D. 1998. Late Cretaceous to early Tertiary subduction history of the Antarctic Peninsula. *Journal of the Geological Society, London*, **155**, 255–268, https://doi.org/10.1144/gsjgs.155.2.0255

McCarron, J.J. and Smellie, J.L. 1998. Tectonic implications of fore-arc magmatism and generation of high-magnesian andesites: Alexander Island, Antarctica. *Journal of the Geological Society, London*, **155**, 269–280, https://doi.org/10.1144/gsjgs.155.2.0269

Nell, P. and Storey, B. 1991. Strike-slip tectonics within the Antarctic Peninsula fore-arc. International Symposium on Antarctic Earth Sciences, Cambridge, **5**, 443–448.

Riley, T.R. and Leat, P.T. 2021. Palmer Land and Graham Land volcanic groups (Antarctic Peninsula): petrology. *Geological Society, London, Memoirs*, **55**, 139–156, https://doi.org/10.1144/M55-2018-51

Riley, T.R., Flowerdew, M.J. and Haselwimmer, C.E. 2011. *Geological Map of Eastern Graham Land, Antarctic Peninsula*. sheet 1 edn. 1:625 000. BAS GEOMAP 2 Series. British Antarctic Survey, Cambridge.

Riley, T.R., Burton-Johnson, A., Flowerdew, M.J. and Whitehouse, M.J. 2018. Episodicity within a mid-Cretaceous magmatic flare-up in West Antarctica: U–Pb ages of the Lassiter Coast intrusive suite, Antarctic Peninsula, and correlations along the Gondwana margin. *Geological Society of America Bulletin*, **130**, 1177–1196, https://doi.org/10.1130/B31800.1

Riley, T.R., Flowerdew, M.J., Burton-Johnson, A., Leat, P.T., Millar, I.L. and Whitehouse, M.J. 2020. Cretaceous arc volcanism of Palmer Land, Antarctic Peninsula: zircon U-Pb geochronology, geochemistry, distribution and field relationships. *Journal of Volcanology and Geothermal Research*, **401**, 106969, https://doi.org/10.1016/j.jvolgeores.2020.106969

Salze, M., Martinod, J., Guillaume, B., Kermarrec, J.-J., Ghiglione, M.C. and Sue, C. 2018. Trench-parallel spreading ridge subduction and its consequences for the geological evolution of the overriding plate: insights from analogue models and comparison with the Neogene subduction beneath Patagonia. *Tectonophysics*, **737**, 27–39, https://doi.org/10.1016/j.tecto.2018.04.018

Siegert, M.J. 2008. Antarctic subglacial topography and ice-sheet evolution. *Earth Surface Processes and Landforms*, **33**, 646–660, https://doi.org/10.1002/esp.1670

Spiegel, C., Kohn, B., Belton, D., Berner, Z. and Gleadow, A. 2009. Apatite (U–Th–Sm)/He thermochronology of rapidly cooled samples: the effect of He implantation. *Earth and Planetary Science Letters*, **285**, 105–114, https://doi.org/10.1016/j.epsl.2009.05.045

Stegman, D., Freeman, J., Schellart, W., Moresi, L. and May, D. 2006. Influence of trench width on subduction hinge retreat rates in 3-D models of slab rollback. *Geochemistry, Geophysics, Geosystems*, **7**, Q03012, https://doi.org/10.1029/2005GC001056

Stevens Goddard, A.L. and Fosdick, J.C. 2019. Multichronometer thermochronologic modeling of migrating spreading ridge subduction in southern Patagonia. *Geology*, **47**, 555–558, https://doi.org/10.1130/G46091.1

Storey, B.C. and Nell, P.A.R. 1988. Role of strike-slip faulting in the tectonic evolution of the Antarctic Peninsula. *Journal of the Geological Society, London*, **145**, 333–337, https://doi.org/10.1144/gsjgs.145.2.0333

Storey, B.C., Brown, R.W., Carter, A., Doubleday, P.A., Hurford, A.J., Macdonald, D.I.M. and Nell, P.A.R. 1996*a*. Fission-track evidence for the thermotectonic evolution of a Mesozoic–Cenozoic fore-arc, Antarctica. *Journal of the Geological Society, London*, **153**, 65–82, https://doi.org/10.1144/gsjgs.153.1.0065

Storey, B.C., Vaughan, A.P.M. and Millar, I.L. 1996*b*. Geodynamic evolution of the Antarctic Peninsula during Mesozoic times and its bearing on Weddell Sea history. *Geological Society, London, Special Publications*, **108**, 87–103, https://doi.org/10.1144/GSL.SP.1996.108.01.07

Thorkelson, D.J. 1996. Subduction of diverging plates and the principles of slab window formation. *Tectonophysics*, **255**, 47–63, https://doi.org/10.1016/0040-1951(95)00106-9

Vaughan, A.P.M. and Storey, B.C. 2000. The eastern Palmer Land shear zone: a new terrane accretion model for the Mesozoic development of the Antarctic Peninsula. *Journal of the Geological Society, London*, **157**, 1243–1256, https://doi.org/10.1144/jgs.157.6.1243

Vaughan, A.P.M., Kelley, S.P. and Storey, B.C. 2002. Mid-Cretaceous ductile deformation on the Eastern Palmer Land Shear Zone, Antarctica, and implications for timing of Mesozoic terrane collision. *Geological Magazine*, **139**, 465–471, https://doi.org/10.1017/S0016756802006672

Vaughan, A.P.M., Eagles, G. and Flowerdew, M.J. 2012. Evidence for a two-phase Palmer Land event from crosscutting structural relationships and emplacement timing of the Lassiter Coast Intrusive Suite, Antarctic Peninsula: implications for mid-Cretaceous Southern Ocean plate configuration. *Tectonics*, **31**, 1–19, https://doi.org/10.1029/2011tc003006

Vermeesch, P., Seward, D., Latkoczy, C., Wipf, M., Günther, D. and Baur, H. 2007. α-Emitting mineral inclusions in apatite, their effect on (U–Th)/He ages, and how to reduce it. *Geochimica et Cosmochimica Acta*, **71**, 1737–1746, https://doi.org/10.1016/j.gca.2006.09.020

Wellner, J.S., Anderson, J.B., Ehrmann, W., Weaver, F.M., Kirshner, A., Livsey, D. and Simms, A.R. 2011. History of an evolving ice sheet as recorded in SHALDRIL cores from the northwestern Weddell Sea, Antarctica. *In:* Anderson, J.B. and Wellner, J.S. (eds) *Tectonic, Climatic, and Cryospheric Evolution of the Antarctic Peninsula*, **63**, 131–152, https://doi.org/10.1029/2010SP001047